of Laboratory Animal Resources (Washington, DC, USA). To create a parkinsonian model, the monkey was injected intravenously with 1-methyl-4-phenyl-1,2,3,6-tetrahydropyridine (MPTP) HCl (0.4 mg/kg as a free base; Sigma–Aldrich) twice a week until we observed persistent parkinsonian symptoms, such as tremor, bradykinesia, and impaired balance. Stable parkinsonian symptoms were observed for more than 12 weeks before the animal was used for the experiments. The coordinates of the targets were obtained using MRI, and human iPSC-derived NPCs were stereotactically transplanted into the bilateral putamen of the MPTP-treated monkey (d28 spheres on the right side, d42 spheres on the left side). The sphere suspension was prepared at 1×10^5 cells/μl, and 1 μl of this suspension was injected along six tracts on each side (four injection sites/tract; 4.8×10^6 cells/animal). After surgery, the monkey was given antibiotics for three days and a daily intravenous immunosuppressant (FK506, 0.05 mg/kg; Astellas Pharma) until sacrifice. Average trough values of circulating FK506 were 14.0 ng/ml ($n = 3$). Five-week-old male NOD/ShiJic-scid/Jcl mice (CLEA Japan) were also used as transplant recipients. Using a 26-gauge needle, each mouse received a stereotactic injection of 1 μl of cell solution (253G4-derived cells: 1×10^5 cells/μl) in the right side of the striatum (from the Bregma: A +0.5, L +1.8, V +3.0, incisor bar 0). Six months after transplantation, the animals were sacrificed and analyzed.

MRI

T1- and T2-weighted images were obtained using a 3-Tesla MRI scanner (Siemens Healthcare) and an 8-channel receiving coil (see Supplementary Methods for details of the MRI scans). Graft volume was analyzed using Functional Magnetic Resonance Images of Brain (FMRIB) Software Libraries [13]. In T1- and T2-weighted images, nonbrain structures were removed using the Brain Extraction Tool [14] and were coregistered with each other based on rigid body transformation using FMRIB's Linear Registration Tool [15]. Next, to identify the graft region, we subjected T1- and T2-weighted images to automated segmentation using the Fast Automated Segmentation Tool [16], which is based on a hidden Markov random field model and an associated expectation–maximization algorithm. We segmented and searched a multichannel set of T1- and T2-weighted images of different tissue types. This process reproducibly identified white matter, gray matter, cerebrospinal fluid (CSF) space (plus graft region, if any), and putamen. Next, partial volume images for the CSF plus graft were thresholded at 30%, binarized, and manually edited to remove the CSF region. The resulting segment image of the graft was used to calculate the graft volume.

PET

A bolus of 6-[^{18}F]fluoro-L-3,4-dihydroxyphenylalanine ([^{18}F]DOPA), [^{11}C]dihydrotetrabenazine ([^{11}C]DTBZ), (*E*)-*N*-(3-iodoprop-2-enyl)-2β-carbo [^{11}C]methoxy-3β-(4-methylphenyl)nortropane ([^{11}C] PE2I), or 3′-deoxy-3′-[^{18}F]fluorothymidine ([^{18}F] FLT) (37 MBq/kg in 2.0 ml of saline) was intravenously delivered within 10 sec under anesthesia via continuous infusion of propofol (10–20 mg/kg/hr). For [^{18}F]DOPA PET scans, a solution of carbidopa (10 mg/kg) was administered intravenously 5 min prior to the scan to minimize peripheral decarboxylation of [^{18}F]DOPA. PET images were acquired using a microPET Focus-220 system (Siemens Healthcare) with a scan duration of 90 min in three-dimensional list mode (see Supplementary Methods for preparation steps and image analysis). The axial and transaxial resolutions of the PET scanner were 1.35 mm at full-width half-maximum. Transmission scanning was performed for 30 min with a rotating 68Ge-68Ga pin source (18.5 MBq) to determine the attenuation factor for image reconstruction just before an emission scan. PET images of [^{18}F]FLT summed over 60 min (30–90 min after the injection) were converted into standardized uptake values and used for further imaging analysis. To determine anatomic locations, PET images were coregistered onto magnetic resonance images using a three-dimensional rigid-body alignment program from image analysis software (PMOD).

Behavioral analysis

The behavior of the monkey was evaluated according to a previously described rating scale for monkey PD models [6]. The normal and minimum score is 0, whereas the maximum total score is 24. The evaluation was performed by a trained examiner who was not involved in the cell transplantation procedure. Spontaneous movements were measured as previously described [17]. Video records were analyzed using the Vigie Primates video-based analysis system (View Point, Lyon, France), and changes in pixels from one image to the next were counted every 66.67 ms. Movements were categorized into one of three levels

based on the number of pixel changes per 66.67 ms (large: more than 501 pixels; medium: 101 to 500 pixels; small: less than 100 pixels). The total time spent making each type of movement was then determined. During the raisin pick-up test, the monkey was placed in a special cage with a small slit through which it could pick up a raisin placed 20 cm from the cage. During a single session, the monkey reached for 20–24 raisins (10–12 raisins on each side).

Dopamine release assay

Accutase (Innovative Cell Technologies) was used to dissociate d28 spheres into small pieces, which were cultured on poly-L-ornithine/laminin–coated culture dishes with neurobasal/B-27 media containing BDNF, GDNF, dbcAMP, and ascorbic acid. Fourteen days later, cells were washed twice with low-concentration KCl solution (20 mM HEPES-NaOH at pH 7.4, 140 mM NaCl, 4.7 mM KCl, 2.5 mM $CaCl_2$, 1.2 mM $MgSO_4$, 1.2 mM KH_2PO_4, and 11 mM glucose) and incubated in the low-concentration KCl solution for 2 min. The medium was subsequently replaced with 1 ml of high-concentration KCl solution (20 mM HEPES-NaOH at pH 7.4, 85 mM NaCl, 60 mM KCl, 2.5 mM $CaCl_2$, 1.2 mM $MgSO_4$, 1.2 mM KH_2PO_4, and 11 mM glucose) and the samples were incubated for 15 min. The solution was then collected and the dopamine concentration was determined using high-performance liquid chromatography (HPLC), including a reverse-phase column and an electrochemical detector system (HTEC-500, Eicom, Japan). Data were obtained from three independent experiments.

Flow cytometry

Cells were harvested on day 14 using Accumax, gently dissociated into single-cell suspensions, and resuspended in phenol-free HBSS (Gibco) containing 1% bovine serum albumin and 0.03% NaN_3. Samples were filtered through cell strainer caps (35-μm mesh; BD Biosciences) and subjected to surface marker staining using anti-PSA-NCAM antibodies (Chemicon). Primary antibodies were added, the samples were incubated at 4°C for 30 min, and the cells were washed twice with HBSS buffer. Secondary antibodies were then added and the samples were incubated at 4°C for 30 min. Dead cells and debris were excluded based on 7-AAD staining. Analyses were performed using a FACSAriaII cell sorter and FACSDiva software (BD Biosciences).

Statistical analysis

Statistical analyses were performed using a commercially available software package (GraphPad Prism, GraphPad Software). Data were analyzed using one-factor ANOVA and Tukey's post-hoc analysis, except for the raisin pick-up test (Fig. 6E; Student's *t*-tests). Differences were considered statistically significant when $P<0.05$ ($^{*}P<0.05$, $^{**}P<0.01$, or $^{***}P<0.001$).

RESULTS

Neural differentiation from human iPSCs using serum-free floating cultures

To generate NPCs, we cultured human iPSCs (253G4) [9] as floating spheres in serum-free medium, such that the cell suspension (9000 cells/well) formed one sphere in each well (Fig. 1A). On day 7, the spheres contained primarily $Pax6^+$ neuroepithelial cells (Fig. 1B) and a small number of $Oct3/4^+$ cells (Fig. 1C). On day 14, almost all cells were immunopositive for both Nestin and Pax6 (Fig. 1D), whereas a small population expressed Tuj1 (Fig. 1E) and no $Oct3/4^+$ or $Nanog^+$ cells were observed (data not shown). Furthermore, flow cytometric analysis on day 14 detected the neural cell surface marker PSA-NCAM on $99.8 \pm 0.1\%$ of the cells (Fig. 1F), indicating that the cells were committed to a neural lineage. We then replaced the culture medium with neurobasal medium, and continued the floating culture in the presence or absence of Shh and FGF8. After a 2-week expansion period (days 14–28), immunocytochemistry revealed that most of the cells were $Tuj1^+$ and $3.14 \pm 1.38\%$ of them were TH^+ on day 28 (Fig. 1G, H, K). Next, we removed Shh and FGF8, and added BDNF, GDNF, ascorbic acid, and dbcAMP to promote maturation of DA neurons. After another 2-week expansion period (days 28–42), the percentage of TH^+ DA neurons among the $Tuj1^+$ neurons in the spheres increased to $85.46 \pm 3.13\%$ (Fig. 1I–K). Quantitative RT-PCR analyses revealed that expression of undifferentiated cell markers (Oct3/4, Nanog) decreased, whereas expression of neural cell markers (Sox1, Pax6) markedly increased between days 0 and 14 (Fig. 1L; supplementary Figure 1). Between days 14 and 42, expression levels of TH gradually increased, indicating that the cells moved to a DA fate. Together with neural differentiation, expression levels of introduced genes (Sox2, Klf4) increased slightly, whereas c-Myc expression did not markedly change (supplementary Figure 1). Based

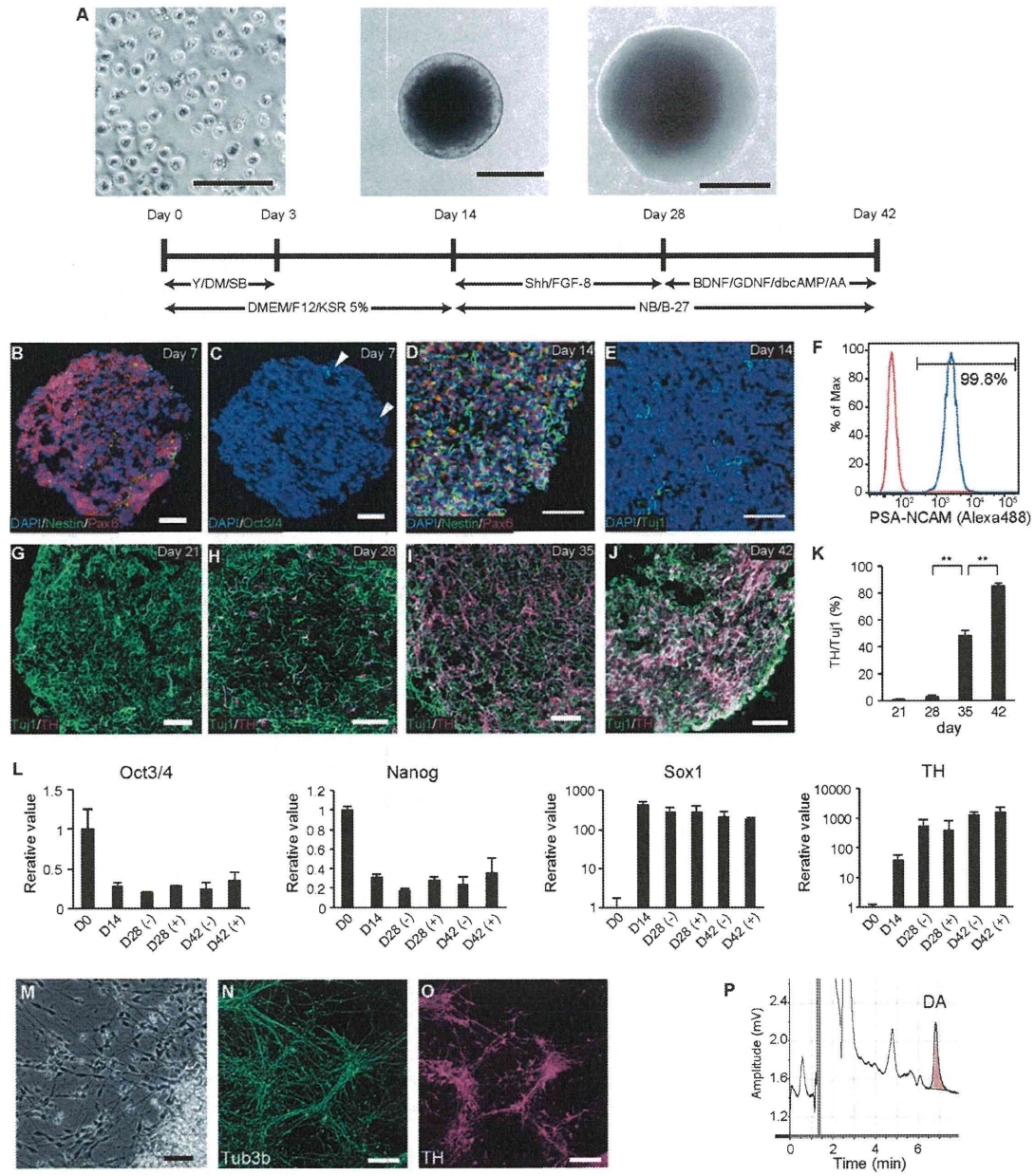

Fig. 1. Neural differentiation using human iPSCs in floating culture. (A) Protocol for the feeder-free floating culture with phase-contrast images of the cells or spheres on days 0, 14, and 28. (B–E) Double- or triple-immunolabeled d7 spheres (B and C) or d14 spheres (D and E). In B and D, Nestin and Pax6 labeling is shown in green and magenta, respectively. In C, Oct3/4 labeling is represented by green, whereas Tuj1 labeling is denoted in green in E. Scale bars, 100 μm. (F) Fluorescence-activated cell sorting analysis of the expression of the neural cell marker PSA-NCAM on day 14. The red line denotes the negative control samples. (G–J) Double-immunolabeled spheres on days 21 (G), 28 (H), 35 (I), and 42 (J). Tuj1 labeling and TH labeling are shown in green and magenta, respectively. Scale bars, 50 μm. (K) Percentages of TH^+ cells among the $Tuj1^+$ cells. Data are presented as means ± SEM (**$P < 0.001$, ANOVA). (L) Time-course analysis of pluripotent cell ($Oct3/4^+$, $Nanog^+$), NPC ($Sox1^+$), and DA neuron (TH^+) markers using quantitative RT-PCRs. Expression levels in iPSCs before differentiation (D0) were set to 1, and the relative expression levels are presented as means ± SEM. Samples were incubated with (+) or without (–) Shh and FGF8 between day 14 and day 28. (M) Phase-contrast and (N, O) immunofluorescence images of differentiated iPSCs on poly-L-ornithine/laminin–coated slides. Scale bars, 50 μm. (P) HPLC analysis showing dopamine release in culture medium containing differentiated iPSCs following KCl-evoked depolarization.

on these results, we compared spheres obtained on day 28 (d28 spheres) and day 42 (d42 spheres) in *in vivo* experiments.

To assess the development of the human iPSC-derived NPCs in our neural differentiation system, we induced DA maturation by culturing d28 spheres on poly-L-ornithine/laminin–coated slides in the presence of BDNF, GDNF, ascorbic acid, and dbcAMP. Two weeks later, the cells extended Tuj1$^+$ neurites and most cells were TH$^+$ (Fig. 1M–O). In addition, HPLC revealed that the cells secreted dopamine into the culture medium in response to high potassium concentrations (196 ± 138 pg/ml; Fig. 1P). Thus, our system produced functional DA neurons from human iPSCs without feeder cells.

Graft growth in NOD-SCID mice

We then compared growth and DA cell differentiation in d28 and d42 spheres in the brains of NOD-SCID mice. Spheres with or without Shh and FGF8 treatment (days 14–28; Fig. 1A) were grafted into the right striatum, and the animals were subjected to immunohistologic studies at 6 months. Grafts derived from d28 spheres (d28 grafts) were significantly larger than d42 grafts (Fig. 2A, B, E). iPSC-derived TH$^+$ cells were observed in these grafts, which also expressed the midbrain DA neuron marker Nurr1 (Fig. 2C, D). Significantly more TH$^+$ cells were observed in d28 grafts without Shh and FGF8 treatment than in d42 grafts with Shh and FGF8 treatment (Fig. 2F), although no significant differences were noted for TH$^+$ cell density in the grafts (Fig. 2G).

Graft growth in an MPTP-treated monkey

We grafted d28 and d42 spheres into the right and left putamina, respectively, of an MPTP-treated cynomolgus monkey (Fig. 3A). Six months after transplantation, MRI showed that grafted cells survived and proliferated in the monkey brain (Fig. 3B). Because MRI of the grafts matched results obtained from H–E staining of brain slices (supplementary Figure 2), we used MRI to measure graft sizes in each tract (Fig. 3C, supplementary Figure 3). For d28 grafts, cells treated with Shh and FGF8 resulted in significantly larger grafts ($172.25 \pm 3.07\,mm^3$, $P < 0.001$) than those obtained with untreated d28(–) cells ($39.21 \pm 6.18\,mm^3$). In contrast, d42 grafts were significantly smaller than d28(+) grafts, and did not significantly differ based on Shh and FGF8 treatment ($19.36 \pm 8.28\,mm^3$ and $22.79 \pm 9.72\,mm^3$ with and without Shh and FGF8, respectively). Between 3 and 6 months, the average doubling times of the d28 grafts with and without Shh and FGF8 were 101 days and 257 days, respectively, whereas those of the d42 grafts were 271 days (the L4 graft was omitted because it stopped expanding) and 148 days, respectively (supplementary Figure 3). In each case, the doubling time between 3 and 6 months post-transplantation was longer than that observed between 1 and 3 months, indicating that the grafts were expanding more slowly. PET with [^{18}F]FLT—a fluorinated thymidine analog—has been previously used to evaluate cell proliferation, for example, in the diagnosis of malignant brain tumors [18]. In this study, however, focal uptake of [^{18}F]FLT was not observed in the 6 months after transplantation (Fig. 3D), and standard uptake values in representative grafts ranged between 0.04 and 0.11 (Fig. 3E). Based on an average standard uptake value of 0.12 in the preoperative monkey, these values were relatively low.

H–E staining showed more cell accumulation in d28 grafts (Fig. 4A) than in d42 grafts (Fig. 4D). In addition, immunohistochemical analyses revealed more Vimentin$^+$ cells and fewer Nestin$^+$ cells in d28 grafts (Fig. 4B, C) than in d42 grafts (Fig. 4E, F). Interestingly, these immature cells were located in the graft core. The percentage of cells expressing Ki67, a marker of proliferating cells, was significantly higher in d28 grafts than in d42 grafts ($0.84 \pm 0.02\%$ vs. $0.23 \pm 0.13\%$; Fig. 4G). Ki67$^+$ cells in d28 grafts were also immunopositive for Vimentin (Fig. 4I), indicating that immature neural or mesenchymal cells were proliferating. In contrast, Ki67$^+$ cells in the d42 grafts were also Nestin$^+$ (Fig. 4H), indicating that some of the grafted cells were still NPCs and a few were proliferating.

DA activity in grafts in an MPTP-treated monkey

Next, we examined *in vivo* differentiation of the grafted cells. TH$^+$ cells were located in the periphery of each graft (Fig. 5A, B), and the density of TH$^+$ cells was higher in d42 grafts treated with Shh and FGF8 (Fig. 5C, D; supplementary Figure 4). The total number of TH$^+$ cells was 3.07×10^4 and 1.26×10^5 in right and left side, respectively (Fig. 5C, supplementary Figure 4). These TH$^+$ cells also expressed markers for mature midbrain DA neurons, including Nurr1, VMAT2, DAT, Girk2, and Pitx3 (Fig. 5E–I). The results suggest that d42 spheres treated with Shh and FGF8 efficiently generated midbrain DA neurons in the monkey brain. Dopamine synthesis, vesicle transport, and dopamine reuptake can be visualized in PET studies using [^{18}F]DOPA, [^{11}C]DTBZ, and [^{11}C]PE2I,

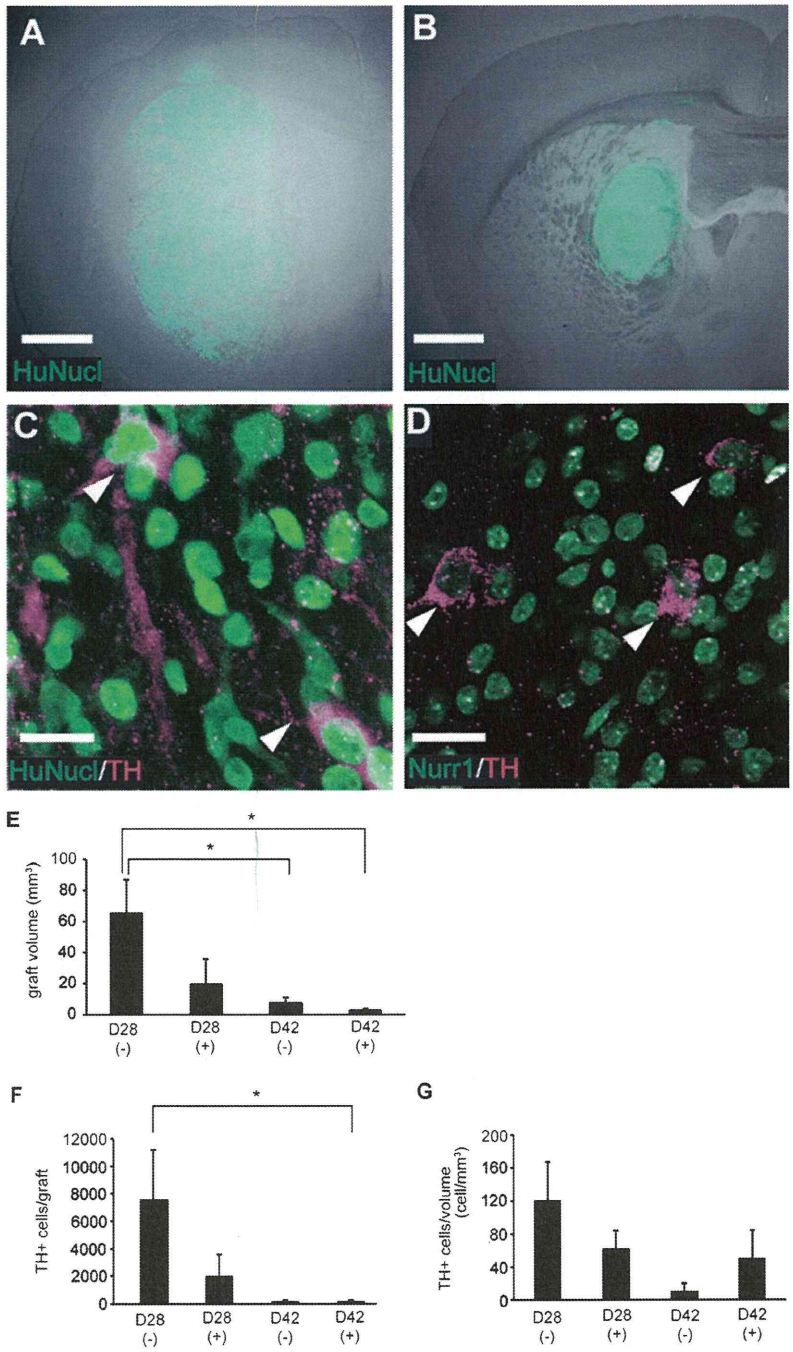

Fig. 2. Growth and differentiation of human iPSC-derived NPCs in mouse brains. (A, B) Representative immunofluorescence images of d28 (A) and d42 (B) grafts with Shh and FGF8 treatment. Human nuclei are labeled green. Scale bars, 1 mm. (C, D) Representative TH^+ cells (red) in these grafts, expressing a human nucleus-specific antigen (green in C) or the midbrain DA neuron marker Nurr1 (green in D). Scale bars, 20 μm. (E–G) Graft volume (E), number of TH^+ cells/graft (F), and number of TH^+ cells/mm^3 (G) in each condition are presented as means ± SEM (*$P < 0.05$, ANOVA; $n = 4$ and 7 for d28 grafts, 5 and 6 for d42 grafts with (+) or without (−) Shh and FGF8 treatment, respectively). All mice were sacrificed and analyzed at 6 months after transplantation.

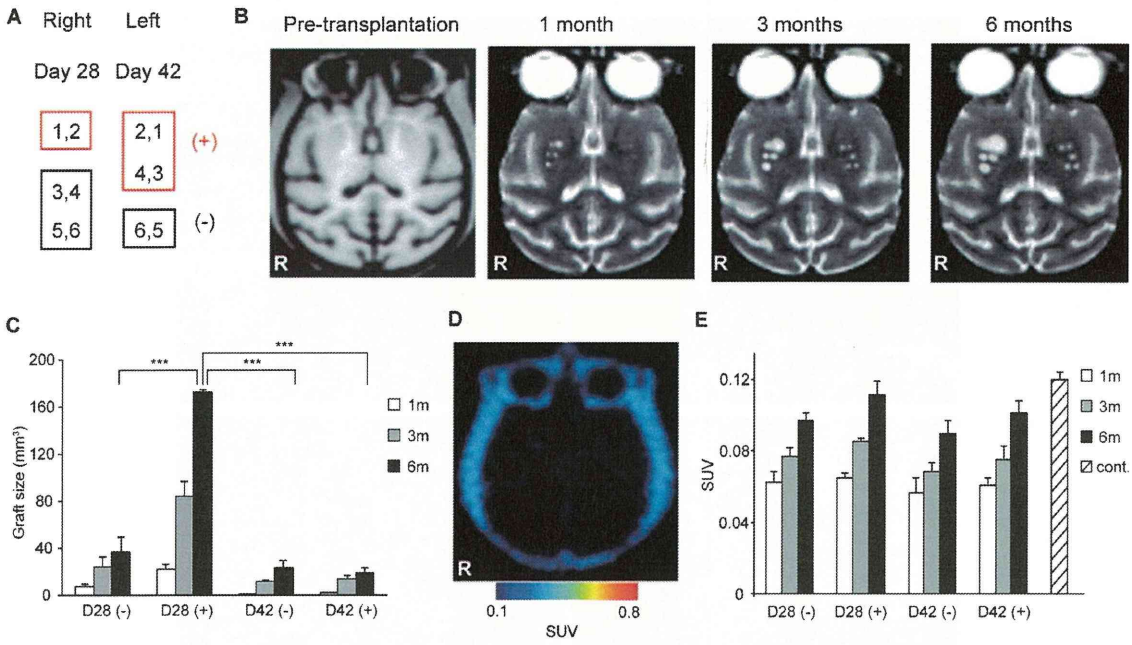

Fig. 3. Growth of NPCs in a MPTP-treated monkey brain. (A) Schematic of the positions of the grafted cells with (+) or without (−) Shh and FGF8 treatment. (B) Axial magnetic resonance images of the monkey before and 1, 3, and 6 months after transplantation. (C) Graft volumes at 1, 3, and 6 months are presented as means ± SEM (***$P < 0.001$, ANOVA). (D) A [^{18}F]FLT-PET image obtained at 6 months after transplantation. (E) Standard uptake values obtained with [^{18}F]FLT-PET at 1, 3, and 6 months after transplantation are presented as means ± SEM. The striped bar represents the average value from preoperative controls ($n = 3$).

respectively [19, 20]. [^{18}F]DOPA-PET at 6 months after transplantation revealed higher Ki values in the d28 grafts, especially those treated with Shh and FGF8 (Fig. 5J, M). This, however, may be a false-positive result owing to detection of 3-O-methyl-6-[^{18}F]fluoro-L-DOPA (OMFD; see discussion). In [^{11}C]DTBZ-PET and [^{11}C]PE2I-PET, ligand binding in the anterior putamen was relatively low (Fig. 5K, L). This finding in the MPTP-treated monkey mirrors the pathology of PD in humans, which is initially characterized by impaired posterodorsal innervations [20]. Intriguingly, the binding potential of [^{11}C]PE2I increased after cell transplantation in d42(+) grafts, suggesting DA cell differentiation from the grafted NPCs (Fig. 5L, M).

Finally, we evaluated the behaviors of the MPTP-treated monkey before and after NPC transplantation. We employed a previously described behavioral rating scale [6], and observed a slight improvement 6 months after transplantation (Fig. 6A). We also performed video-based analysis [17] of spontaneous movements by the monkey. The percentages of time spent making large- and medium-sized movements before transplantation were 0.8% and 7.1%, respectively. Six months later, the time spent making these types of movement increased to 1.0% and 8.9%, respectively (Fig. 6B). The total amount of movement—measured based on changes in video pixels during a 30-min period—also increased after transplantation (898,690 to 995,642 affected pixels; Fig. 6C, D). To distinguish between the effects in the right and left hemispheres, we performed a video-based analysis of the monkey picking up a raisin. We measured the duration of time spent reaching, grasping, and retracting with each arm (supplementary Figure 5). After 6 months, the monkey grasped the raisin and retracted the right arm more quickly (Fig. 6E). Although we did not detect a statistically significant difference, the observed results may reflect more surviving DA neurons in the left striatum.

DISCUSSION

In this study, we used NOD-SCID mice and an MPTP-treated monkey to characterize transplanted human iPSC-derived NPCs. Our results show that human iPSCs incubated in feeder-free floating culture generated functional midbrain DA neurons. Moreover, only NPCs pretreated with Shh and FGF-8 followed by

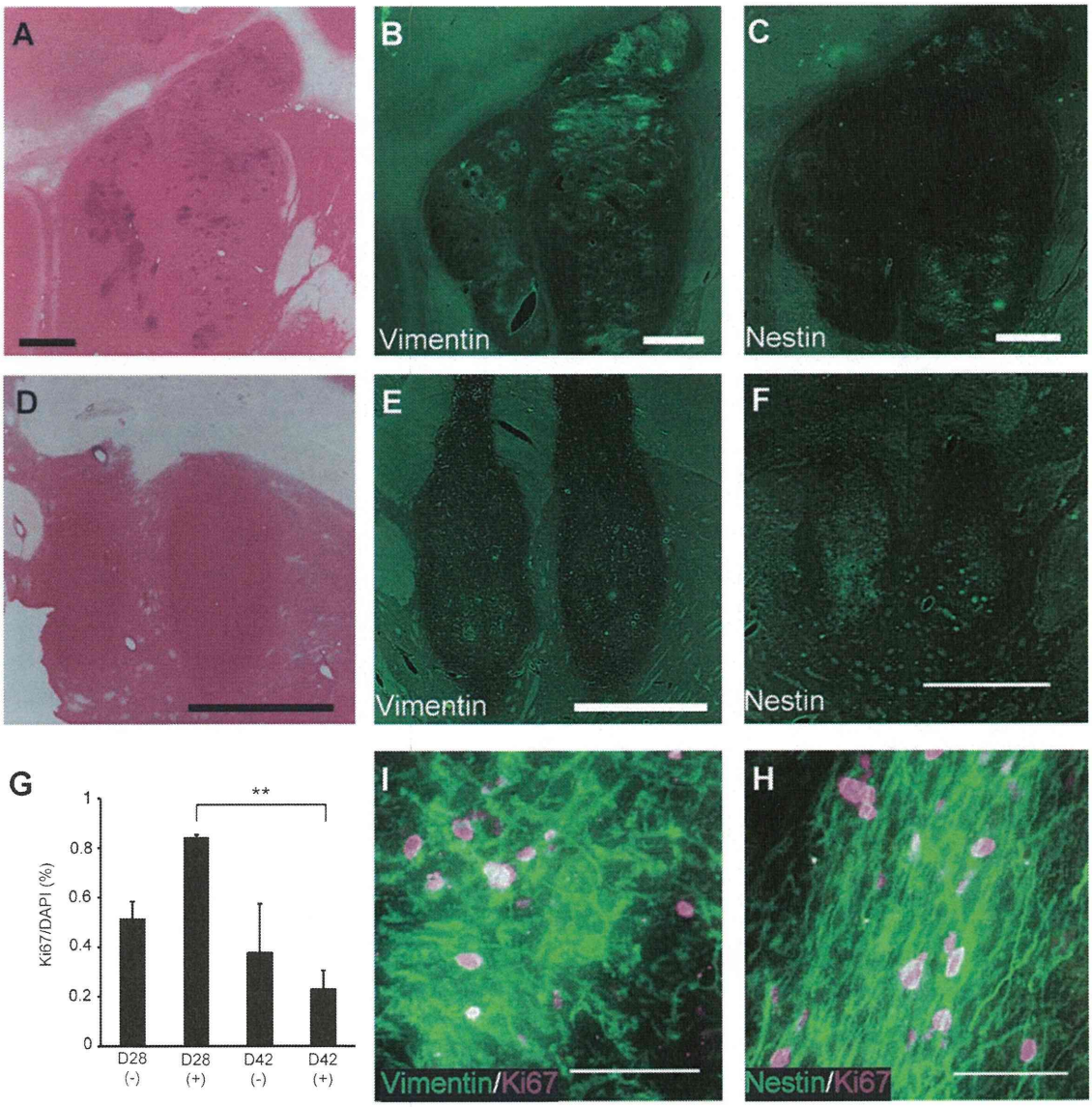

Fig. 4. Expression of immature cell markers in the grafts. (A) H–E staining and (B, C) immunofluorescence images of d28 grafts. Scale bars, 2 mm. (D) H–E staining and (E, F) immunofluorescence images of d42 grafts. Scale bars, 2 mm. (G) Percentages of $Ki67^+$ cells among total cells are presented as means ± SEM (**$P < 0.01$, ANOVA). (I, H) Immunofluorescence images showing labeling of Ki67 (magenta) and Vimentin (green in I) or Nestin (green in H). Scale bars, 50 μm.

GDNF, BDNF, ascorbic acid, and dbcAMP resulted in a substantial number of functional DA neurons in the monkey's brain. Finally, MRI and PET allowed real-time monitoring of *in vivo* cell proliferation and activity.

In two recent studies, midbrain DA neurons were induced to develop from human iPSCs, but the method required coculture with mouse stromal feeder cells [1, 2]. Our feeder-free differentiation method would be more suitable if the cells are to be used clinically. Our mouse and monkey studies demonstrated that d28 spheres resulted in larger grafts at 6 months, suggesting that some NPCs remained immature and proliferated in the brain. These results were consistent with a previous study showing that human embryonic stems cells that differentiated into neurons on PA6 stromal feeder

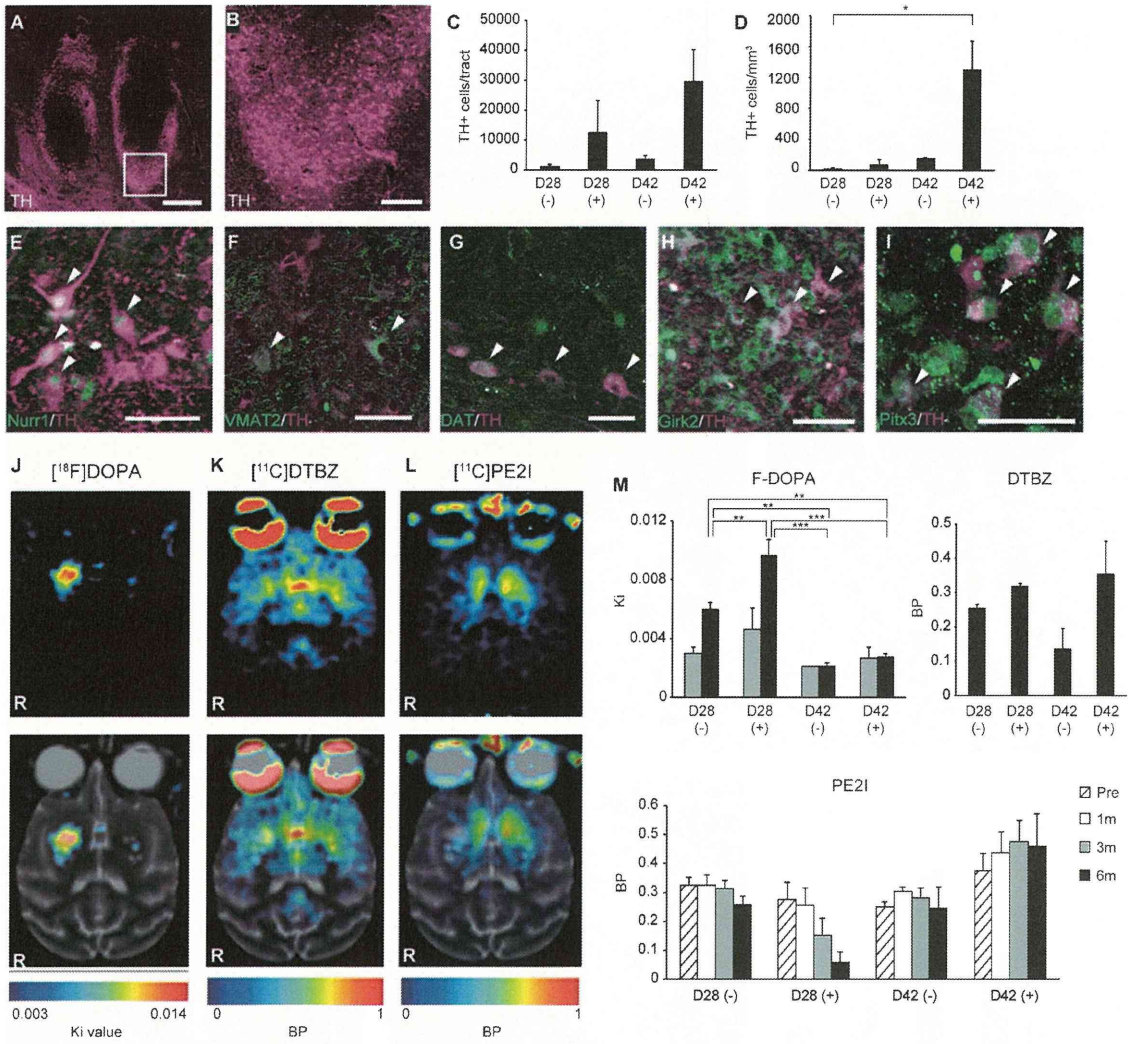

Fig. 5. DA neuron differentiation from grafted NPCs in a monkey brain. (A, B) Immunofluorescence images of d42 grafts stained for TH at 6 months after transplantation. A magnified image of the area denoted in (A) is shown in (B). Scale bars, 1 mm in (A) and 200 μm in (B). (C) The number of TH^+ cells/graft, and (D) number of TH^+ cells/mm^3 are presented as means ± SEM. (*$P < 0.05$, ANOVA) (E–I) Immunofluorescence images showing labeling of TH (magenta) and Nurr1 (green in E), VMAT2 (green in F), DAT (green in G), Girk2 (green in H), or Pitx3 (green in I). Scale bars, 50 μm. (J–L) T2-weighted magnetic resonance images with overlapping data obtained using [^{18}F]DOPA-PET (J), [^{11}C]DTBZ-PET (K), or [^{11}C]PE2I-PET (L) at 6 months after transplantation. (M) Ki values ([^{18}F]DOPA) and binding potentials ([^{11}C]DTBZ, [^{11}C]PE2I) at the indicated time points are presented as means ± SEM (*$P < 0.05$, **$P < 0.01$, ***$P < 0.001$, ANOVA).

cells were less tumorigenic as the differentiation period increased [21]. The proliferating NPCs in the d28 spheres also generated TH^+ cells in the graft, whereas TH^+ cells in d42 spheres did not survive in the mouse brains probably because of issues related to xenografts between human and mice.

In contrast to the mouse studies, d42 spheres generated a substantial number of DA neurons in the monkey brain. Furthermore, treatment with Shh and FGF8 followed by BDNF and GDNF was required to generate mature DA neurons. As discussed above, d28 spheres that resulted in continuous proliferation of $Vimentin^+$ and $Nestin^+$ cells were too immature to generate mature DA neurons in the brain when such neurotrophic factors as BDNF and GDNF were absent. These results are consistent with

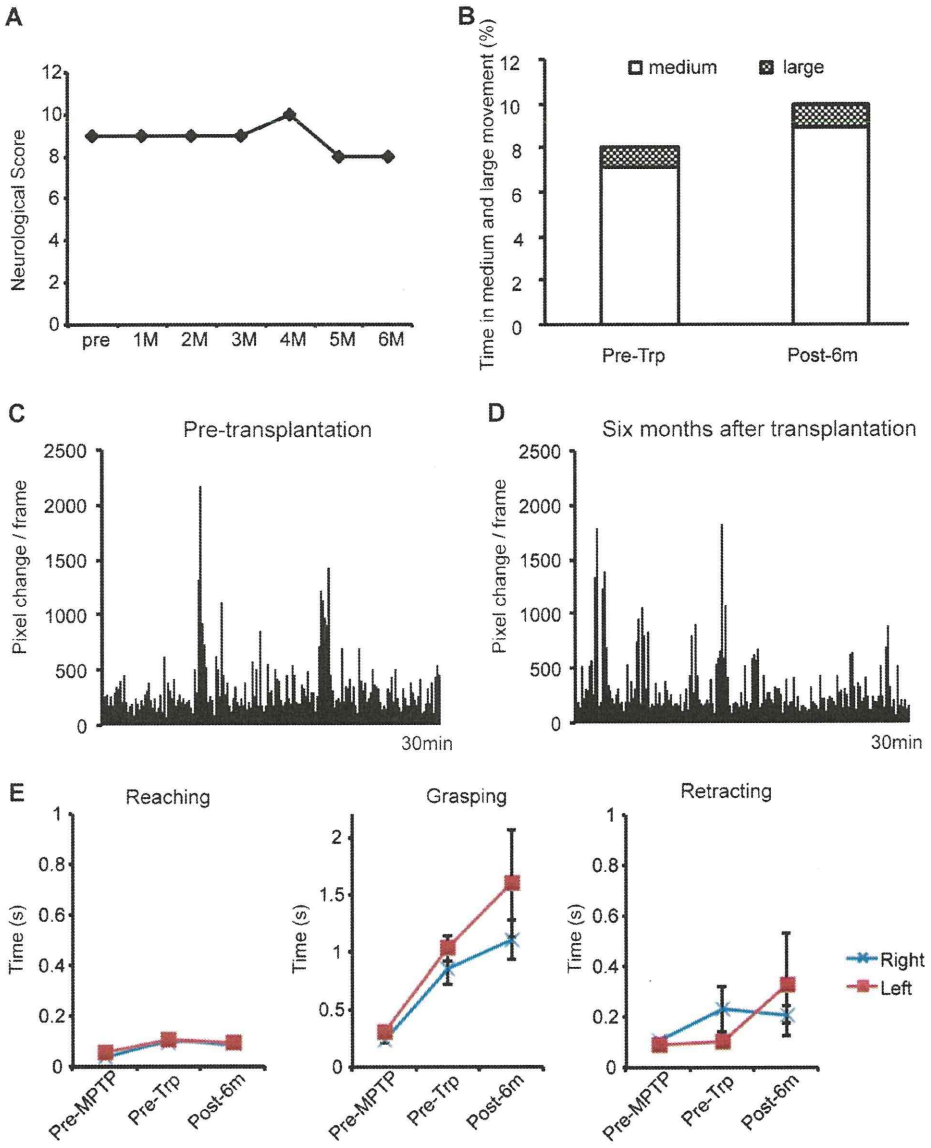

Fig. 6. Neurologic function in an MPTP-treated monkey. (A) Neurologic scores for the monkey before and after cell transplantation. (B) Percentage of time spent making medium or large movements before and 6 months after transplantation. The rest of the time was spent making small movements. (C, D) Pixel changes in each 66.67-ms time period based on spontaneous movements of the monkey during a 30-min trial. (E) Time spent reaching, grasping, and retracting in a raisin pick-up test. Data are presented as the means ± SEM ($P > 0.05$, Student's t test).

previous studies showing good survival of DA neurons in allografts derived from mouse embryonic stem cells [12] and monkey embryonic tissues [22] undergoing neurogenesis into DA neurons. Intriguingly, d28 spheres treated with Shh and FGF8 produced larger grafts, which may reflect maintenance of $Pax6^+$ rosette-forming neuroepithelial cells by Shh and FGF8 [23]. Yet even d42 spheres did not provide a perfect donor population, because some $Nestin^+$ cells were still proliferating in the core of the graft 6 months after transplantation. Therefore, safer and more efficient transplantation will require some modification of our approach, such as purifying DA neuron progenitors or promoting DA maturation *in vivo*.

PET has been extensively employed to elucidate functional changes associated with PD, and [^{18}F]DOPA-PET is the gold standard for assessing dopamine synthesis. In this study, however, uptake of [^{18}F]DOPA was much greater in d28 grafts even though they contained only a small number of TH$^+$ cells. The observed uptake may have reflected accumulation of OMFD, a major metabolite of [^{18}F]DOPA that penetrates the blood–brain barrier and accumulates in brain tumors [24]. Thus, high levels of [^{18}F]DOPA uptake in d28 grafts may indicate cell proliferation rather than dopamine synthesis, a particularly relevant consideration for stem cell transplantation. As demonstrated in this study, examining ligands for dopamine synthesis, transport, and reuptake reflects DA activity in the grafted NPCs. Furthermore, these approaches can also be used in human patients.

Patients with PD who received fetal cell grafts required at least 100,000 TH$^+$ cells in each putamen to achieve good clinical responses [5]. Because the monkey putamen is one-tenth the size of the human putamen [25, 26], we estimated that 10,000 cells were needed for a monkey to recover from neurologic deterioration. Thus, the d42 grafts in this study should have contained a sufficient number of TH$^+$ cells (150,000 in total). Furthermore, some of the TH$^+$ cells that were located in the periphery region expressed Pitx3$^+$ and Girk2$^+$, suggesting that they were A9 DA neurons and able to innervate striatum [27]. Behavioral improvements, however, were moderate in this study. This may reflect insufficient maturation of the majority of TH$^+$ cells or differentiation to an inappropriate fate (namely, into diencephalic or olfactory bulb DA neurons). The follow-up period post-transplantation may have been too short to allow the human neurons to functionally integrate into the brain. Alternatively, functional synapses may not form well in this xeno-transplantation model. Finally, the remaining NPCs or other cell types in the graft (e.g., GABA neurons) may have suppressed the function of the iPSC-derived DA neurons.

In conclusion, we have successfully induced the development of DA neurons using a feeder-free culture method. Moreover, the cells survived for 6 months in the brain of a primate PD model. A substantial number of DA neurons were obtained from d42 spheres treated with Shh and FGF8 followed by BDNF and GDNF. We also developed a system to evaluate the transplanted cells using MRI and PET, behavioral analyses, and histologic examinations, all of which will be useful in preclinical research. Additional studies using other primate models and NPCs subjected to alternative pretreatment protocols will help elucidate the therapeutic potential of human iPSCs.

ACKNOWLEDGMENTS

We thank Drs. K. Takahashi and S. Yamanaka (Kyoto University, Center for iPS Cell Research and Application) for providing human iPSCs, Dr. Y. Ono (KAN Research Institute) for anti-Nurr1 antibodies, Drs. T. Yamamoto and H. Magotani (Shin Nippon Biomedical Laboratories) for their help with the monkey, Astellas Pharma for FK506, and Mr. K. Kubota and Ms. M. Katsukawa in our laboratory for their technical assistance. This study was supported by the following grants: a grant from the Project for Realization of Regenerative Medicine from the MEXT, and a Health and Labor Sciences Research Grant for Research on Regenerative Medicine for Clinical Application. The authors declare that they have no competing interests.

REFERENCES

[1] Wernig M, Zhao JP, Pruszak J, Hedlund E, Fu D, Soldner F, Broccoli V, Constantine-Paton M, Isacson O, & Jaenisch R (2008) Neurons derived from reprogrammed fibroblasts functionally integrate into the fetal brain and improve symptoms of rats with Parkinson's disease. *Proc Natl Acad Sci U S A*, **7**, 7.

[2] Hargus G, Cooper O, Deleidi M, Levy A, Lee K, Marlow E, Yow A, Soldner F, Hockemeyer D, Hallett PJ, Osborn T, Jaenisch R, & Isacson O (2010) Differentiated Parkinson patient-derived induced pluripotent stem cells grow in the adult rodent brain and reduce motor asymmetry in Parkinsonian rats. *Proc Natl Acad Sci U S A*, **107**, 15921-15926.

[3] Freed CR, Greene PE, Breeze RE, Tsai WY, DuMouchel W, Kao R, Dillon S, Winfield H, Culver S, Trojanowski JQ, Eidelberg D, & Fahn S (2001) Transplantation of embryonic dopamine neurons for severe Parkinson's disease. *N Engl J Med*, **344**, 710-719.

[4] Olanow CW, Goetz CG, Kordower JH, Stoessl AJ, Sossi V, Brin MF, Shannon KM, Nauert GM, Perl DP, Godbold J, & Freeman TB (2003) A double-blind controlled trial of bilateral fetal nigral transplantation in Parkinson's disease. *Ann Neurol*, **54**, 403-414.

[5] Lindvall O, & Björklund A (2004) Cell therapy in Parkinson's disease. *NeuroRx*, **1**, 382-393.

[6] Takagi Y, Takahashi J, Saiki H, Morizane A, Hayashi T, Kishi Y, Fukuda H, Okamoto Y, Koyanagi M, Ideguchi M, Hayashi H, Imazato T, Kawasaki H, Suemori H, Omachi S, Iida H, Itoh N, Nakatsuji N, Sasai Y, & Hashimoto N (2005) Dopaminergic neurons generated from monkey embryonic stem cells function in a Parkinson primate model. *J Clin Invest*, **115**, 102-109.

[7] Sanchez-Pernaute R, Studer L, Ferrari D, Perrier A, Lee H, Vinuela A, & Isacson O (2005) Long-term survival of dopamine neurons derived from parthenogenetic primate embryonic stem cells (cyno-1) after transplantation. *Stem Cells*, **23**, 914-922.

[8] Redmond DEJ, Bjugstad KB, Teng YD, Ourednik V, Ourednik J, Wakeman DR, Parsons XH, Gonzalez R, Blanchard BC, Kim SU, Gu Z, Lipton SA, Markakis EA, Roth RH, Elsworth JD, Sladek JRJ, Sidman RL, & Snyder EY (2007) Behavioral improvement in a primate Parkinson's model is associated with multiple homeostatic effects of human neural stem cells. *Proc Natl Acad Sci U S A*, **104**, 12175-12180.

[9] Takahashi K, Tanabe K, Ohnuki M, Narita M, Ichisaka T, Tomoda K, & Yamanaka S (2007) Induction of pluripotent stem cells from adult human fibroblasts by defined factors. *Cell*, **131**, 861-872.

[10] Watanabe K, Ueno M, Kamiya D, Nishiyama A, Matsumura M, Wataya T, Takahashi JB, Nishikawa S, Muguruma K, & Sasai Y (2007) A ROCK inhibitor permits survival of dissociated human embryonic stem cells. *Nat Biotechnol*, **25**, 681-686.

[11] Koyanagi M, Takahashi J, Arakawa Y, Doi D, Fukuda H, Hayashi H, Narumiya S, & Hashimoto N (2008) Inhibition of the Rho/ROCK pathway reduces apoptosis during transplantation of embryonic stem cell-derived neural precursors. *J Neurosci Res*, **86**, 270-280.

[12] Morizane A, Doi D, Kikuchi T, Nishimura K, & Takahashi J (2011) Small-molecule inhibitors of bone morphogenic protein and activin/nodal signals promote highly efficient neural induction from human pluripotent stem cells. *J Neurosci Res*, **89**, 117-126.

[13] Smith SM, Jenkinson M, Woolrich MW, Beckmann CF, Behrens TE, Johansen-Berg H, Bannister PR, De Luca M, Drobnjak I, Flitney DE, Niazy RK, Saunders J, Vickers J, Zhang Y, De Stefano N, Brady JM, & Matthews PM (2004) Advances in functional and structural MR image analysis and implementation as FSL. *Neuroimage*, **23**(Suppl 1), S208-S219.

[14] Smith SM (2002) Fast robust automated brain extraction. *Hum Brain Mapp*, **17**, 143-155.

[15] Jenkinson M, & Smith S (2001) A global optimisation method for robust affine registration of brain images. *Med Image Anal*, **5**, 143-156.

[16] Zhang Y, Brady M, & Smith S (2001) Segmentation of brain MR images through a hidden Markov random field model and the expectation-maximization algorithm. *IEEE Trans Med Imaging*, **20**, 45-57.

[17] Saiki H, Hayashi T, Takahashi R, & Takahashi J (2010) Objective and quantitative evaluation of motor function in a monkey model of Parkinson's disease. *J Neurosci Methods*, **190**, 198-204.

[18] Saga T, Kawashima H, Araki N, Takahashi JA, Nakashima Y, Higashi T, Oya N, Mukai T, Hojo M, Hashimoto N, Manabe T, Hiraoka M, & Togashi K (2006) Evaluation of primary brain tumors with FLT-PET: Usefulness and limitations. *Clin Nucl Med*, **31**, 774-780.

[19] Poyot T, Condé F, Grégoire MC, Frouin V, Coulon C, Fuseau C, Hinnen F, Dollé F, Hantraye P, & Bottlaender M (2001) Anatomic and biochemical correlates of the dopamine transporter ligand 11C-PE2I in normal and parkinsonian primates: Comparison with 6-[18F]fluoro-L-dopa. *J Cereb Blood Flow Metab*, **21**, 782-792.

[20] Pavese N, & Brooks DJ (2009) Imaging neurodegeneration in Parkinson's disease. *Biochim Biophys Acta*, **1792**, 722-729.

[21] Brederlau A, Correia AS, Anisimov SV, Elmi M, Paul G, Roybon L, Morizane A, Bergquist F, Riebe I, Nannmark U, Carta M, Hanse E, Takahashi J, Sasai Y, Funa K, Brundin P, Eriksson PS, & Li JY (2006) Transplantation of human embryonic stem cell-derived cells to a rat model of Parkinson's disease: Effect of *in vitro* differentiation on graft survival and teratoma formation. *Stem Cells*, **24**, 1433-1440.

[22] Elsworth JD, Sladek JR, Taylor JR, Collier TJ, Redmond DE, & Roth RH (1996) Early gestational mesencephalon grafts, but not later gestational mesencephalon, cerebellum or sham grafts, increase dopamine in caudate nucleus of MPTP-treated monkeys. *Neuroscience*, **72**, 477-484.

[23] Elkabetz Y, Panagiotakos G, Al Shamy G, Socci ND, Tabar V, & Studer L (2008) Human ES cell-derived neural rosettes reveal a functionally distinct early neural stem cell stage. *Genes Dev*, **22**, 152-165.

[24] Beuthien-Baumann B, Bredow J, Burchert W, uuml F, chtner F, Bergmann R, Alheit HD, Reiss G, Hliscs R, Steinmeier R, Franke WG, Johannsen B, & Kotzerke J (2003) 3-O-methyl-6-[18F]fluoro-L-DOPA and its evaluation in brain tumour imaging. *Eur J Nucl Med Mol Imaging*, **30**, 1004-1008.

[25] Schaltenbrand G, & Wahren W (1997) Atlas for stereotaxy of the human brain, Georg Thieme Verlag, Stuttgart, Germany, plate 17, a.13.5-p.1.5.

[26] Martin RF, & Bowden DM (2000) Primate Brain Maps: Structure of the Macaque Brain, Elsevier Science Ltd, 270-284.

[27] Thompson L, Barraud P, Andersson E, Kirik D, & Bjorklund A (2005) Identification of dopaminergic neurons of nigral and ventral tegmental area subtypes in grafts of fetal ventral mesencephalon based on cell morphology, protein expression, and efferent projections. *J Neurosci*, **25**, 6467-6477.

SUPPLEMENTARY METHODS

MRI scans

Before transplantation, a high-resolution T1-weighted image was obtained for each animal using a fast spoiled gradient-echo (FSPGR) sequence (TR = 7.812 ms, TE = 1.912 ms, TI = 600 ms, FA = 7°, matrix = 128 × 128, field of view (FOV) = 102.4 mm, slice thickness = 0.8 mm), and examined to identify the injection site (posterodorsal striatum) in the grafts. After transplantation, T1-weighted, T2-weighted, and fluid-attenuated-inversion recovery (FLAIR) images were obtained with thicker slices and used to evaluate brain pathology qualitatively with a better signal-to-noise ratio. T1 images were obtained using an FSPGR sequence (TR = 7.504 ms, TE = 1.784 ms, TI = 600 ms, FA = 7°, matrix = 128 × 128, FOV = 100 mm, slice thickness = 2 mm), T2 images were obtained using a fast spin echo sequence (TR = 5400 ms, TE = 101.024, FA = 90°, matrix = 160 × 160, FOV = 100 mm, slice thickness = 2 mm), and FLAIR image were obtained using an inversion recovery sequence (TR = 8502 ms, TE = 83.22 ms, IR = 2800 ms, FA = 90°, matrix = 160 × x160, FOV = 100 mm, slice thickness = 2 mm).

Preparation of PET ligands

[^{11}C]PE2I was prepared by exposing the corresponding free acid precursor (1.2 mg) in

Supplementary Table 1
Real-time RT-PCR primers

Gene Name	Forward	Reverse
Oct3/4	5′- CCCCAGGGCCCCATTTTGGTACC-3′	5′-ACCTCAGTTTGAATGCATGGGAGAGC-3′
Nanog	5′-GGCTCTGTTTTGCTATATCCCCTAA-3′	5′-CATTACGATGCAGCAAATACGAGA-3′
Sox2	5′-TTCACATGTCCCAGCACTACCAGA-3′	5′-TCACATGTGTGAGAGGGGCAGTGTGC-3′
Klf4	5′-CATGCCAGAGGAGCCCAAGCCAAAGAGGGG-3′	5′-CGCAGGTGTGCCTTGAGATGGGAACTCTTT-3′
cMyc	5′-ATACATCCTGTCCGTCCAAGCAGA-3′	5′-ACGCACAAGAGTTCCGTAGCTG-3′
Sox1	5′-GCGGAGCTCGTCGCATT-3′	5′-GCGGTAACAACTACAAAAAACTTGTAA-3′
Pax6	5′-CTGGCTAGCGAAAAGCAACAG-3′	5′-CCCGTTCAACATCCTTAGTTTATCA-3′
TH	5′-GCAGTTCTCGCAGGACATTG-3′	5′-CGGCACCATAGGCCTTCA-3′
β-actin	5′-CACCATTGGCAATGAGCGGTTC-3′	5′-CACCATTGGCAATGAGCGGTTC-3′

Supplementary Table 2
Primary antibodies used for immunofluorescence studies

Antibody	Dilution	Company
mouse anti-Oct3	1 : 100	Santa Cruz Biotechnology
rabbit anti-TH	1 : 200	Millipore Chemicon
mouse anti-TH	1 : 200	Millipore Chemicon
mouse anti-Tuj1	1 :100	Millipore Chemicon
mouse anti-Nestin	1 : 300	Covance Research Products
rat anti-DAT	1 : 1000	Millipore Chemicon
mouse anti-Pax6	1 : 500	Hybridoma Bank
rabbit anti-Pax6	1 : 200	Covance Research Products
rat anti-Nurr1	1 : 1000	A gift from KAN laboratory
rabbit anti-Ki67	1 : 1000	Novocastra
rabbit anti-Girk2	1 : 100	Alomone Labs
rabbit anti-VMAT2	1 : 400	Pel-Freez
goat anti-Nanog	1 : 200	R&D
mouse anti-Vimentin	1 : 500	Millipore Chemicon

dimethylformamide (400 μl) to [^{11}C]-CH_3I produced in a cyclotron (HM12; Sumitomo Heavy Industry, Tokyo, Japan). Precursor and standard PE2I were purchased from PharmaSynth AS (Tartu, Estonia). Radiochemical purities were greater than 95%, and specific activities were 63.8 ± 6.8 GBq/μmol (mean ± SEM) at the time of injection. [^{11}C]DTBZ was prepared by exposing (+)-9-O-desmethyl-α-dihydrotetrabenazine (DTBZ precursor) (0.8 mg) in anhydrous dimethyl sulfoxide (400 μl) to [^{11}C]-CH_3I. Precursor and standard DTBZ were purchased from ABX (Radeberg, Germany). Radiochemical purities were greater than 99.5%, and specific activities were greater than 72.6 GBq/μmol at the time of injection.

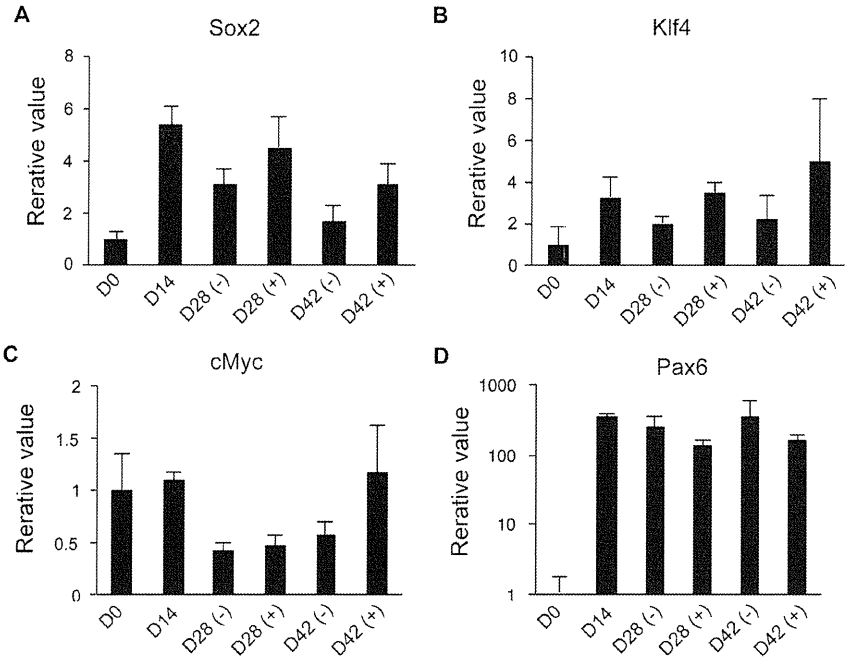

Supplementary Figure 1. Quantitative RT-PCRs to examine the expression of *Sox2* (A), *Klf4* (B), *c-Myc* (C), and *Pax6* (D) in human iPSC-derived spheres.

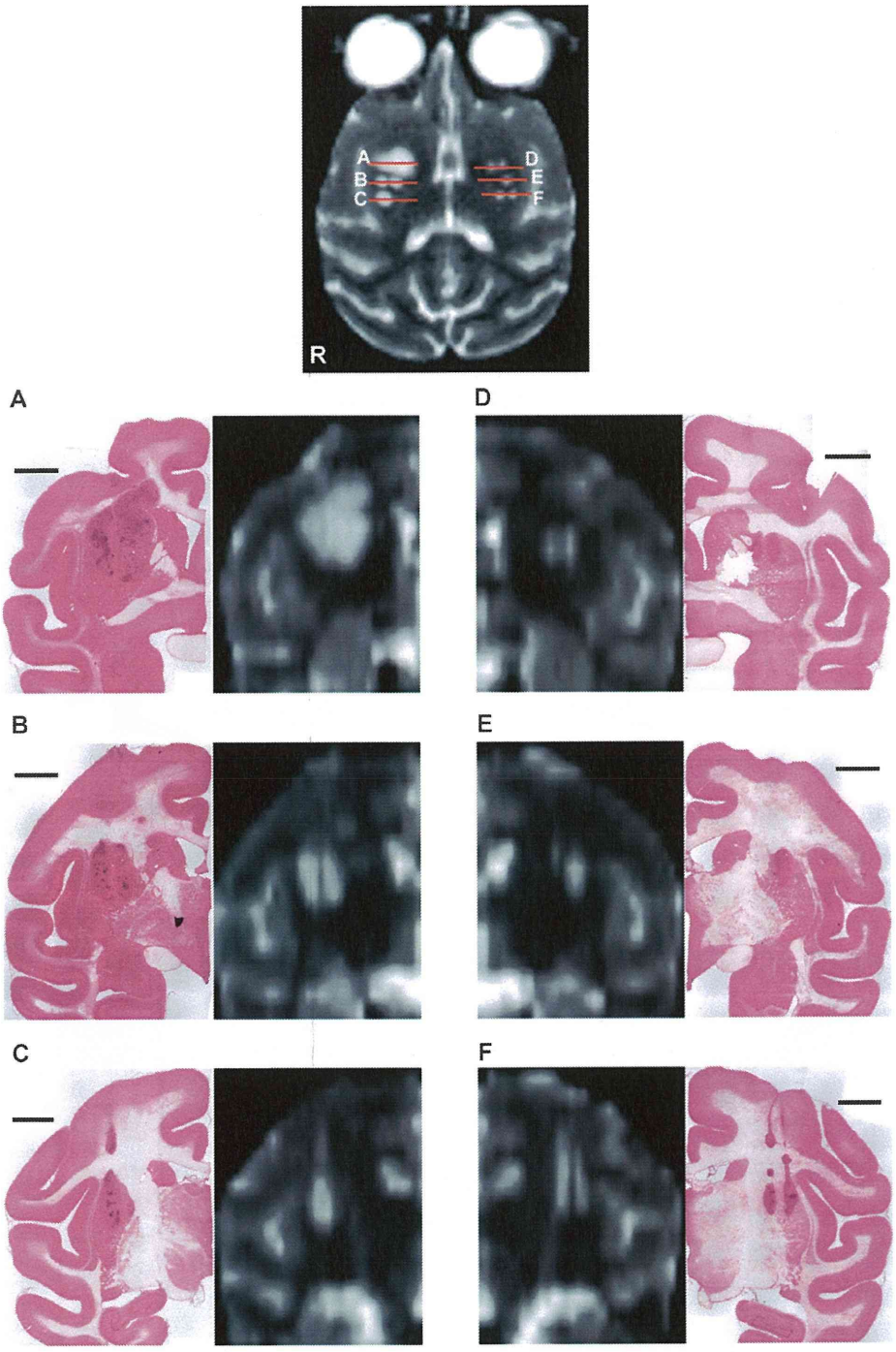

Supplementary Figure 2. A reconstructed T2-weighted magnetic resonance image and H–E staining of identical brain sections (coronal view). Scale bars, 5 mm.

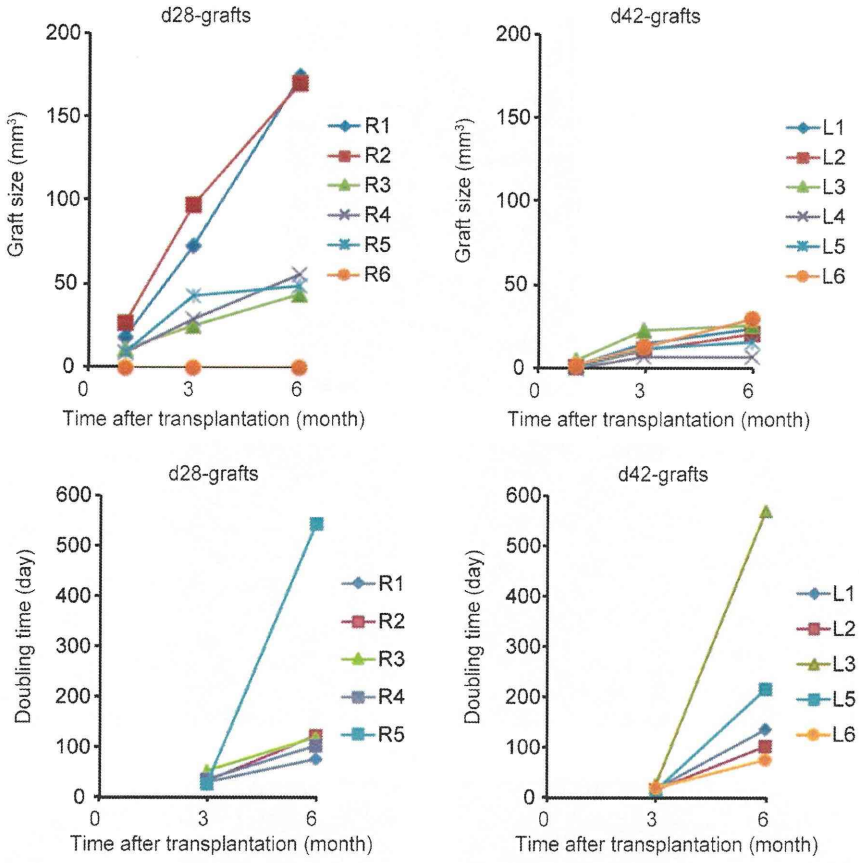

Supplementary Figure 3. Graft size and doubling time in each tract of the iPSC-derived grafts during 1–3 months and 3–6 months post-transplantation. R, right; L, left.

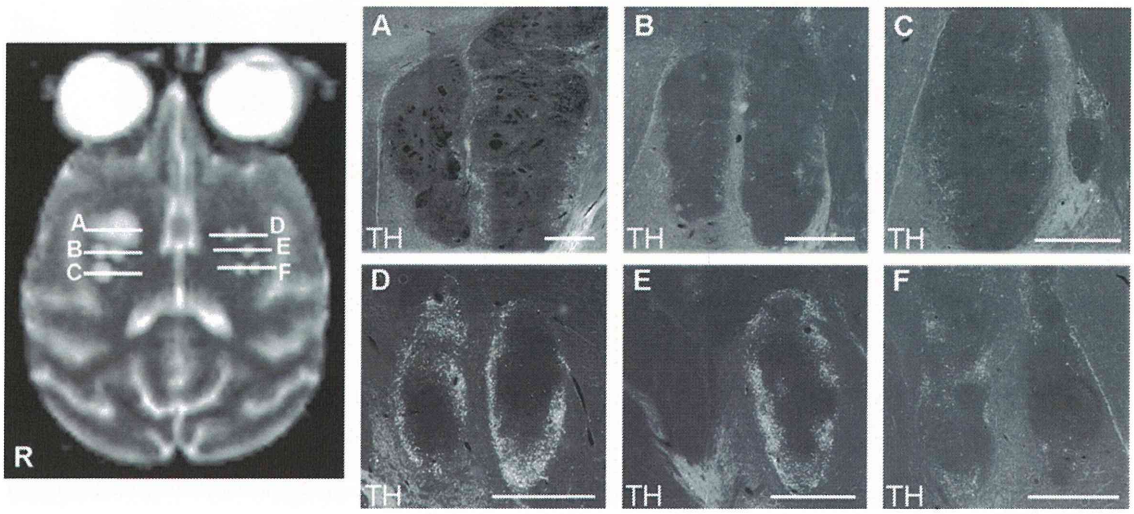

Supplementary Figure 4. Immunofluorescence labeling of tyrosine hydroxylase in each tract of the iPSC-derived grafts 6 months after transplantation. Scale bars, 2 mm. The graphs show the number of TH^+ cells per graft, and per volume (1 mm^3) in each tract.

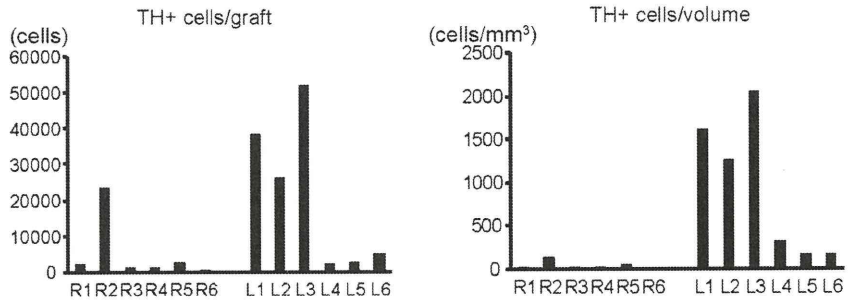

Supplementary Figure 4. *(Continued)*

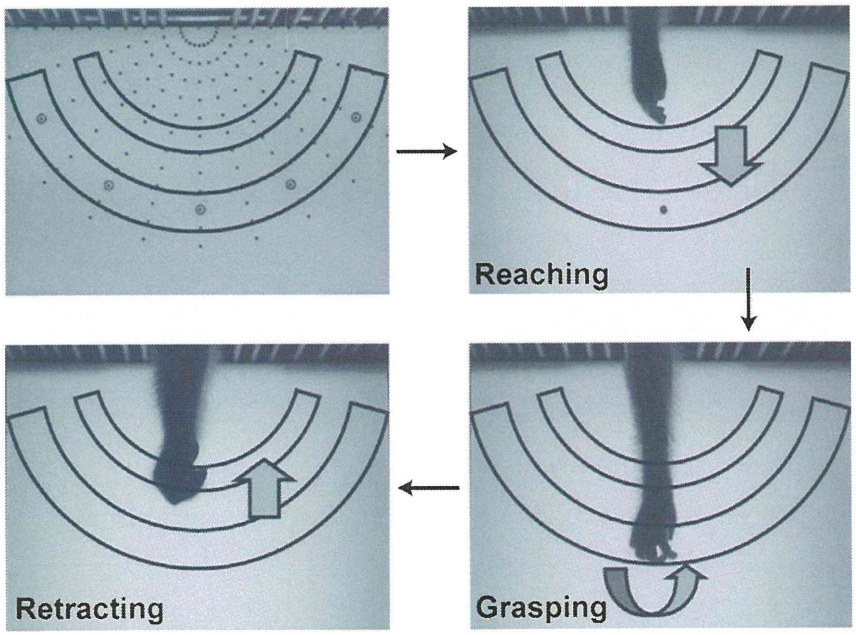

Supplementary Figure 5. Raisin pick-up test. We assessed the time it took for the monkey's hand to move from the first area to the second area (reaching), from the second area to grasp the raisin (grasping), and from the second area to the first area (retracting).

[^{18}F]DOPA and [^{18}F]FLT were synthesized according to previously reported procedures [1, 2].

PET image analysis

[^{18}F]FLT 9PET images obtained for 60 min (30–90 min after the injection) were converted into standardized uptake values to analyze [^{18}F]FLT accumulation. To obtain parametric images, PET results were analyzed using suita ble tracer kinetic models and PMOD software version 3.0 (PMOD Technologies, Adliswil, Switzerland). The examined parameters included uptake rate (Ki, min^{-1}) for [^{18}F]DOPA and the binding potential between the VMAT2 transporter or DA transporter and [^{11}C]DTBZ or [^{11}C]PE2I, respectively. [^{18}F]DOPA Ki was calculated using Patlak graphic analysis, with the cerebellum as the reference region [3]. To quantitate [^{11}C]DTBZ and [^{11}C]PE2I binding in the brain, we calculated binding potentials using the Ichise multilinear reference tissue model [4] and the simplified reference tissue model [5], respectively, with the cerebellum as the reference region. To determine anatomic locations, PMOD software was used to precisely coregister PET and MRI results.

REFERENCES

[1] Ishiwata K, Ishii S-I, Senda M, Tsuchiya Y, & Tomimoto K (1993) Electrophilic synthesis of 6-[18F]fluoro-l-dopa: Use of 4-O-pivaloyl-l-dopa as a suitable precursor for routine production. *Applied Radiation and Isotopes*, **44**, 755-759.

[2] Wodarski C, Eisenbarth J, Weber K, Henze M, Haberkorn U, & Eisenhut M (2000) Synthesis of 3′-deoxy-3′-[18F]fluorothymidine with 2,3′-anhydro-5′-O-(4,4′-dimethoxytrityl)-thymidine. *Journal of Labelled Compounds and Radiopharmaceuticals*, **43**, 1211-1218.

[3] Patlak CS, & Blasberg RG (1985) Graphical evaluation of blood-to-brain transfer constants from multiple-time uptake data Generalizations. *J Cereb Blood Flow Metab*, **5**, 584-590.

[4] Ichise M, Ballinger JR, Golan H, Vines D, Luong A, Tsai S, & Kung HF (1996) Noninvasive quantification of dopamine D2 receptors with iodine-123-IBF SPECT. *J Nucl Med*, **37**, 513-520.

[5] Lammertsma AA, & Hume SP (1996) Simplified reference tissue model for PET receptor studies. *Neuroimage*, **4**, 153-158.